Application of random coherence order selection in gradient-enhanced multidimensional NMR

2016 J. Phys.: Conf. Ser. 699 012004

(http://iopscience.iop.org/1742-6596/699/1/012004)

Journal of Physics: Conference Series **699** (2016) 012004 doi:10.1088/1742-6596/699/1/012004

Application of random coherence order selection in gradient-enhanced multidimensional NMR

Mark J. Bostock and Daniel Nietlispach

Department of Biochemistry, University of Cambridge, 80 Tennis Court Road, Old Addenbrooke's Site, Cambridge CB2 1GA

E-mail: dn206@cam.ac.uk

Abstract. Development of multidimensional NMR is essential to many applications, for example in high resolution structural studies of biomolecules. Multidimensional techniques enable separation of NMR signals over several dimensions, improving signal resolution, whilst also allowing identification of new connectivities. However, these advantages come at a significant cost. The Fourier transform theorem requires acquisition of a grid of regularly spaced points to satisfy the Nyquist criterion, while frequency discrimination and acquisition of a pure phase spectrum require acquisition of both quadrature components for each time point in every indirect (non-acquisition) dimension, adding a factor of 2^{N-1} to the number of free-induction decays which must be acquired, where N is the number of dimensions. Compressed sensing (CS) ℓ_1-norm minimisation in combination with non-uniform sampling (NUS) has been shown to be extremely successful in overcoming the Nyquist criterion. Previously, maximum entropy reconstruction has also been used to overcome the limitation of frequency discrimination, processing data acquired with only one quadrature component at a given time interval, known as random phase detection (RPD), allowing a factor of two reduction in the number of points for each indirect dimension (Maciejewski et al. 2011 *PNAS* **108** 16640). However, whilst this approach can be easily applied in situations where the quadrature components are acquired as amplitude modulated data, the same principle is not easily extended to phase modulated (P-/N-type) experiments where data is acquired in the form $\exp(i\omega t)$ or $\exp(-i\omega t)$, and which make up many of the multidimensional experiments used in modern NMR. Here we demonstrate a modification of the CS ℓ_1-norm approach to allow random coherence order selection (RCS) for phase modulated experiments; we generalise the nomenclature for RCS and RPD as random quadrature detection (RQD). With this method, the power of RQD can be extended to the full suite of experiments available to modern NMR spectroscopy, allowing resolution enhancements for all indirect dimensions; alone or in combination with NUS, RQD can be used to improve experimental resolution, or shorten experiment times, of considerable benefit to the challenging applications undertaken by modern NMR.

1. Introduction

NMR spectroscopy and MRI both suffer limitations due to the measurement time required. In the context of high-resolution biomolecular NMR, this requires samples to be highly concentrated and stable over the length of the measurement, properties which may be mutually exclusive. NMR experiments may be defined as "sampling limited" or "sensitivity limited" [1]. In the former, the length of the experiment is determined by the need to sample multiple indirect dimensions, often to high resolution; in this situation, signal-to-noise is ample, and so time is spent acquiring points on a Nyquist grid to achieve appropriate resolution in the various indirect

(non-acquisition) dimensions. In the sensitivity limited regime, it is the sample concentration which is limiting and so many repetitions of the experiment are needed to achieve appropriate signal-to-noise. In fact, the two regimes are often overlapping; for a given amount of available measurement time (typically a maximum of one week on most high resolution spectrometers due to the need to replace cryogens after this time) the requirement to acquire high resolution and multiple indirect dimensions limits the maximum number of scans and hence the signal-to-noise, while the need to achieve sufficient signal-to-noise for assignment may lead to reductions in resolution. In this region, which is typically the case for studies of large biomolecular systems, such as membrane proteins [2, 3, 4] and protein complexes [5, 6], NMR measurements are usually a trade-off between resolution and sensitivity leading to poor quality spectra, which are hard to assign. Higher dimensional experiments, which could otherwise be extremely beneficial for large molecular systems, are usually inaccessible.

A significant step towards alleviating such problems can be achieved by using time-domain undersampling. Such sparse or non-uniform sampling approaches (NUS) were demonstrated in the early days of multidimensional NMR as an alternative to acquisition of the full Nyquist grid, which requires points to be acquired at $\frac{1}{SW(\mathrm{Hz})}$ where SW is the maximum spectral width in each indirect dimension [7, 8]. In the NUS regime it is no longer possible to use the Fourier transform (FT) to reconstruct frequency domain data and as such, a range of different reconstruction approaches have been developed which include, amongst others, non-uniform Fourier transform [9, 10, 11, 12], maximum entropy (MaxEnt) reconstruction [7, 13, 14], multi-dimensional decomposition [15, 16], SIFT [17] and a range of techniques which reconstruct projections through the various indirect dimensions for example G-matrix Fourier transform NMR [18] and projection-reconstruction NMR [19].

Recently, a new class of reconstructions, inspired by compressed sensing (CS) theory [20, 21, 22], has been developed [23, 24]. Such methods may be convex, based on ℓ_1-norm reconstruction and typically implemented using algorithms such as iterative hard (IHT) or soft (IST) thresholding [24, 25, 26] or non-convex methods such as iteratively-reweighted least squares (IRLS) reconstruction which reduces the norm during the reconstruction i.e. $\ell_{p\rightarrow 0}$-norm reconstruction [24, 27]. More recent developments may allow the use of a range of minimisation functions within a given algorithmic framework [28].

To date CS reconstruction has been applied to NUS data allowing improvements in resolution or sensitivity whilst maintaining accurate intensity reconstruction even in high dynamic range spectra [23, 24, 25, 26]. In addition to the requirement to sample to high resolution, which may be alleviated by NUS based approaches, the other major contribution to the length of NMR experiments is the requirement for frequency discrimination. This is typically achieved via quadrature detection; acquiring two orthogonal phases for each time point. An alternative approach, time-proportional phase incrementation (TPPI) [29], requires oversampling by a factor of two in each indirect dimension. In either case, the effect of frequency discrimination is to increase the number of acquired free induction decays (FIDs) by 2^{N-1} where N is the dimensionality.

Reducing the number of frequency discrimination points would reduce the sampling limitation, allowing sampling to higher resolution for a given experiment time or, in cases where there is ample sensitivity, reduce the experiment time. This can be achieved using the property of randomness, allowing single phase detection, with random selection of either the real or imaginary component. Like NUS data, spectra recorded with random frequency discrimination can be processed with the discrete Fourier transform (DFT) if missing points are replaced with zeros, however this introduces significant artifacts. Consequently, alternative reconstruction approaches may be used to suppress such artifacts. Application of MaxEnt has been demonstrated where the data is recorded according to the States protocol [30], which results in the two quadrature components represented by cosine and sine modulated datasets,

each of which generates an absorption mode spectrum. This approach is known as random phase detection (RPD) and is equivalent to recording 0° or 90° phase components [31]. CS processing of such spectra suppresses artifacts in a similar manner to MaxEnt.

However, many modern NMR experiments use gradient coherence order selection to improve data quality e.g. for improved water suppression or to increase signal-to-noise via sensitivity enhanced and TROSY implementations. The two quadrature points are P- and N-type data of the form (ignoring relaxation)

$$\begin{aligned} \exp(i\Omega_S t_1)\exp(i\Omega_I t_2) \quad &\text{(P-type)} \\ \exp(-i\Omega_S t_1)\exp(i\Omega_I t_2) \quad &\text{(N-type)} \end{aligned}$$

where I and S represent proton and heteronuclear magnetisation and t_2 and t_1 represent the direct and indirect dimensions respectively.

Unlike amplitude modulated data, FT of each individual echo/anti-echo dataset generates signals with the unfavourable phase-twist lineshape [32]. The desired pure phase absorption mode lineshape is achieved by a combination of the two datasets to generate cosine and sine modulated data, which can then be combined via the States routine to generate a purely absorptive spectrum [33].

Clearly for a P-/N-type dataset, randomly acquiring either the P- or N- component, which we name random coherence selection (RCS), cannot be handled by standard reconstruction methods due to the intense artifacts arising from the phase-twist lineshape. Consequently, a modification of the processing method is required. In this paper we demonstrate adaption of the CS-IHT algorithm [25] to process P-/N-type RCS-data (CS-RCS). Given the prevalence of gradient-selected experiments in modern NMR this is a decisive improvement. For both forms of frequency discriminated data, amplitude and phase modulated, RCS and/or RPD may be combined with NUS allowing optimisation of the experimental setup for the high resolution required in modern NMR.

2. Theory

Consider a system of linear equations

$$\mathbf{A}\mathbf{x} = \mathbf{b} \tag{1}$$

where $\mathbf{A}$ is an $M \times N$ matrix and $\mathbf{x}$ is a vector of length N to be recovered from measurements $\mathbf{b}$ where $M < N$. In the context of NMR, $\mathbf{A}$ is the inverse Fourier transform, $\mathbf{b}$ is the time-domain data and $\mathbf{x}$ is the frequency domain spectrum. Where $M < N$, i.e. the data is undersampled, equation (1) has infinitely many solutions. However, CS theory states that $\mathbf{x}$ can be recovered almost exactly if $\mathbf{x}$ is sufficiently sparse by minimising the ℓ_1-norm

$$\min_{\mathbf{x}} ||\mathbf{x}||_1 \text{ subject to } \mathbf{A}\mathbf{x} = \mathbf{b} \tag{2}$$

where

$$||\mathbf{x}||_1 = \sum_i |x_i| \tag{3}$$

For NMR spectra which contain noise, equation (2) is relaxed to

$$\min_{\mathbf{x}} ||\mathbf{x}||_1 \text{ subject to } ||\mathbf{A}\mathbf{x} - \mathbf{b}||_2 \leq \delta \tag{4}$$

CS requires (i) sparse representation of the signal (in a given basis, not necessarily the frequency domain) and (ii) incoherent sampling with respect to that basis. This translates into randomising the sampling schedule, which has been shown to benefit other sampling approaches [34].

Gradient coherence selection experiments produce P- and N-type data of the form

$$\begin{aligned} \exp(i\Omega_S t_1)\exp(i\Omega_I t_2) \quad &\text{(P-type)} \\ \exp(-i\Omega_S t_1)\exp(i\Omega_I t_2) \quad &\text{(N-type)} \end{aligned}$$

In contrast to amplitude modulated data, P- and N-type data shows frequency discrimination, but produces an undesirable phase-twist lineshape [32]. In order to produce an absorption mode lineshape, P- and N-type data (S_P and S_N) is combined to give cosine and sine modulated data ($S_{\cos}$ and $S_{\sin}$) as follows

$$\begin{aligned} S_{\cos}(t_1,t_2) &= (S_P + S_N)/2 \\ S_{\sin}(t_1,t_2) &= (S_P - S_N)/2i \end{aligned}$$

For amplitude modulated data, in order to remove the 2^{N-1} factor resulting from the requirement for frequency discrimination, RPD may be used [31]. Although such methods can be demonstrated for 1D spectra, the benefit of both RPD and NUS-based methods is clearly only realised when recording more than one dimension as such higher or indirect dimensions require a separate FID to be recorded for each time-increment or quadrature-detection point. For a two dimensional experiment, a matrix of hypercomplex points, $\mathbf{z}$, is recorded, represented according to hypercomplex notation as [31, 35]

$$z_{k_1,k_2} = x_{k_1,k_2} + i_1 y_{k_1,k_2} + i_2 r_{k_1,k_2} + i_1 i_2 s_{k_1,k_2} \tag{5}$$

where

$$\begin{aligned} i_1^2 = i_2^2 &= -1 \\ i_1 \cdot i_2 &= i_2 \cdot i_1 \end{aligned} \tag{6}$$

Typically in a 2D experiment, only the indirect dimension would be undersampled giving

$$z_k^{\mathrm{RPD}} = \begin{cases} x_{k_1,k_2} + i_1 y_{k_1,k_2} & \text{if } p_k = 0, \\ i_2 r_{k_1,k_2} + i_1 i_2 s_{k_1,k_2} & \text{if } p_k = 1. \end{cases} \tag{7}$$

Although random phase detection assumes collection of only one phase component at each time-point for the indirect dimensions (i.e. a factor of two reduction in the number of points per indirect dimension), both phase components may be detected, or, in combination with an NUS based schedule, neither may be collected.

Amplitude modulated data of this form may be easily reconstructed through existing reconstruction methods such as MaxEnt and CS by replacing missing points with zeros. Clearly each component produces an absorption mode lineshape and selecting cosine or sine components randomly resolves the sign ambiguity, achieving frequency discrimination. In this case the spectrum will contain only one peak but with additional noise-like sampling artifacts. Applying CS (or other reconstructions methods such as MaxEnt [31]) to such time-domain data can recover a largely artifact-free spectrum.

In contrast RCS of P-/N-type data is non-trivial to reconstruct. In a fully-sampled experiment P-/N- data is combined as follows

$$\frac{1}{2}\left(\exp(i\Omega_S t_1)\exp(i\Omega_I t_2) + \exp(-i\Omega_S t_1)\exp(i\Omega_I t_2)\right) = \cos(\Omega_S t_1)\exp(i\Omega_I t_2) \quad (8)$$

$$\frac{1}{2i}\left(\exp(i\Omega_S t_1)\exp(i\Omega_I t_2) - \exp(-i\Omega_S t_1)\exp(i\Omega_I t_2)\right) = \sin(\Omega_S t_1)\exp(i\Omega_I t_2) \quad (9)$$

allowing processing via the States method [30]. However, this clearly requires both P and N points to be present, which in an RCS experiment would not be the case. In order to combine RCS acquisition with CS, it is important that the data matching step in equation (4) $||\mathbf{Ax}-\mathbf{b}||_2$ uses the raw undersampled data i.e. P-/N-points. If converting the data from cosine-/sine-type to P/N-type is represented by a function $\mathbf{I}$ equation (4) may be reformulated as

$$\min_{\mathbf{x}} ||\mathbf{x}|| \text{ subject to } ||\mathbf{AIx}-\mathbf{b}||_2 \leq \delta \quad (10)$$

As with RPD, the P- and N- points must be sampled randomly for each time-increment to prevent aliasing artifacts from the missing points.

3. Results

Figure 1 demonstrates CS reconstruction (Figure 1B) of an RCS version of a 2D [^{1}H,^{15}N]-SOFAST TROSY for the chicken α-spectrin SRC homology 3 (SH3) domain, a 7 kDa, 62 amino acid protein [36] in comparison to the fast Fourier transform (FFT) reconstruction (Figure 1A) of the fully-sampled data. The reconstruction is of high quality, with good recovery of the peak positions as well as the peak shapes and intensities. RCS data for the CS reconstruction was recorded for half the time of the full reconstruction due to the selection of only one of each quadrature detection point in the ^{15}N dimension (i.e. 56 points for RCS, compared to 56 complex points (112 total points) for the full reconstruction). This reduced the experiment time by 50% to 3 min. Consequently, for a given length of experiment, the time-saving from RCS could be used to improve the resolution. Nevertheless, although a 2D provides a useful illustration of the principle, clearly the benefits of this approach come at higher dimensions. Since CS relies on sparsity in the frequency domain, extending a spectrum into higher dimensions increases the sparsity reducing the number of points required to reconstruct the spectrum.

In Figure 2 the benefit of RQD for higher dimensional experiments is evident. Figure 2 shows a ^{1}H,^{13}C-plane from a 3D [^{1}H,^{15}N]-TROSY HNCA for S195A-human factor IX, a 297 amino acid, 33 kDa protein [37]. In Figure 2A, a plane from the fully-sampled FT-reconstructed spectrum is shown recorded with 384 ^{15}N, ^{13}C complex pairs, equivalent to 1536 total points or 16×24 complex points in the ^{15}N and ^{13}C dimensions respectively. This correlates to $t_{\max}$ for ^{15}N and ^{13}C of 9.22 ms and 5.28 ms respectively. In Figure 2B data is acquired with RCS in the constant time ^{15}N dimension recorded using gradient selection (P-/N-type data), and RPD in the ^{13}C dimension recorded as States-TPPI (cosine-/sine- data). Dimensions 2 and 3 are reconstructed with CS-RCS and normal CS respectively. This allows a factor of two reduction in points per indirect dimension, i.e. a total factor of four saving. In this example, the time-saving is used to sample to higher resolution, in this case equivalent to sampling a matrix of 32×48 complex points for ^{15}N and ^{13}C respectively. This results in $t_{\max}$ of 18.44 ms and 10.56 ms for ^{15}N and ^{13}C respectively. The two sampling schedules are compared in Figures 2C and D, with the axes representing total points in each dimension. The considerable improvement in ^{13}C resolution is evident in Figure 2B, for example by the peaks indicated with an arrow.

With sufficient sparsity NUS and RQD may be combined for significant undersampling. In Figure 3, a ^{1}H,^{15}N-plane from a 3D [^{15}N,^{1}H]-TROSY HN(CO)CA for S195A-human factor

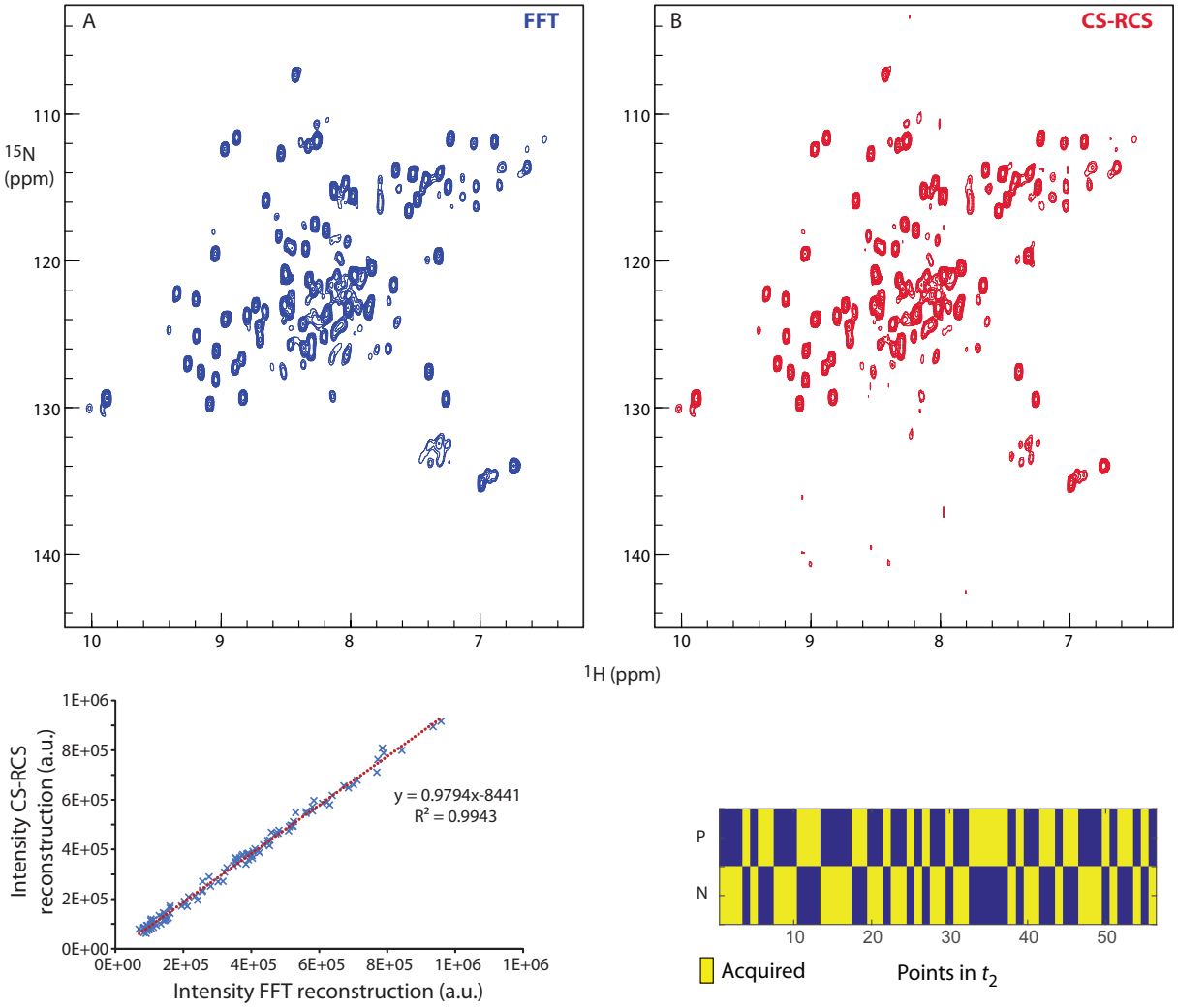

Figure 1. Reconstruction of a 2D [^{1}H,^{15}N]-SOFAST TROSY spectrum for an α-spectrin SH3 domain using FFT reconstruction of fully-sampled data (A) and CS-IHT reconstruction of RCS data (B). The sampling schedule for the RCS data is shown below, with acquired points indicated. 56 points were recorded from total 112 points (56 complex points), i.e. a factor of two reduction in the number of points. The sampled points were selected randomly. Intensities are compared for equivalent peaks picked in the two spectra showing good reproduction of intensities in the CS-RCS reconstruction. The increased noise level in the CS-RCS spectrum results from running the experiment for only half the amount of time of the fully-sampled spectrum. Data was recorded for a 0.3 mM SH3-domain sample at 298 K on a Bruker DRX500 equipped with a 5 mm TCI cryoprobe, with 4 scans, ^{15}N spectral width = 2530.4 Hz and $t_{1\max}$ = 22.1 ms. Recording time for the fully-sampled data was 6 min.

IX is shown. This experiment is recorded with P-/N-type selection in the ^{15}N dimension and amplitude modulation in the ^{13}C dimension. The experiment was acquired using an exponentially weighted NUS schedule recording 350 ^{15}N, ^{13}C pairs from a fully-sampled matrix of 1536 complex pairs, i.e. 22.8% sampling with $t_{1\max}(^{15}N) = 11.52$ ms and $t_{1\max}(^{13}C) = 8.21$ ms. CS reconstruction of the NUS experiment is shown in Figure 3A. Incorporating RCS acquisition with CS-RCS processing in dimension 2 (^{15}N) and RPD acquisition with normal CS-processing in dimension 3 (^{13}C) is shown in Figure 3B. In this case the experiment was undersampled by a further factor of four, equivalent to 5.7% sampling. This equates to an experiment time of approximately 4.5 h. The two sampling schedules for the indirect dimensions are shown below.

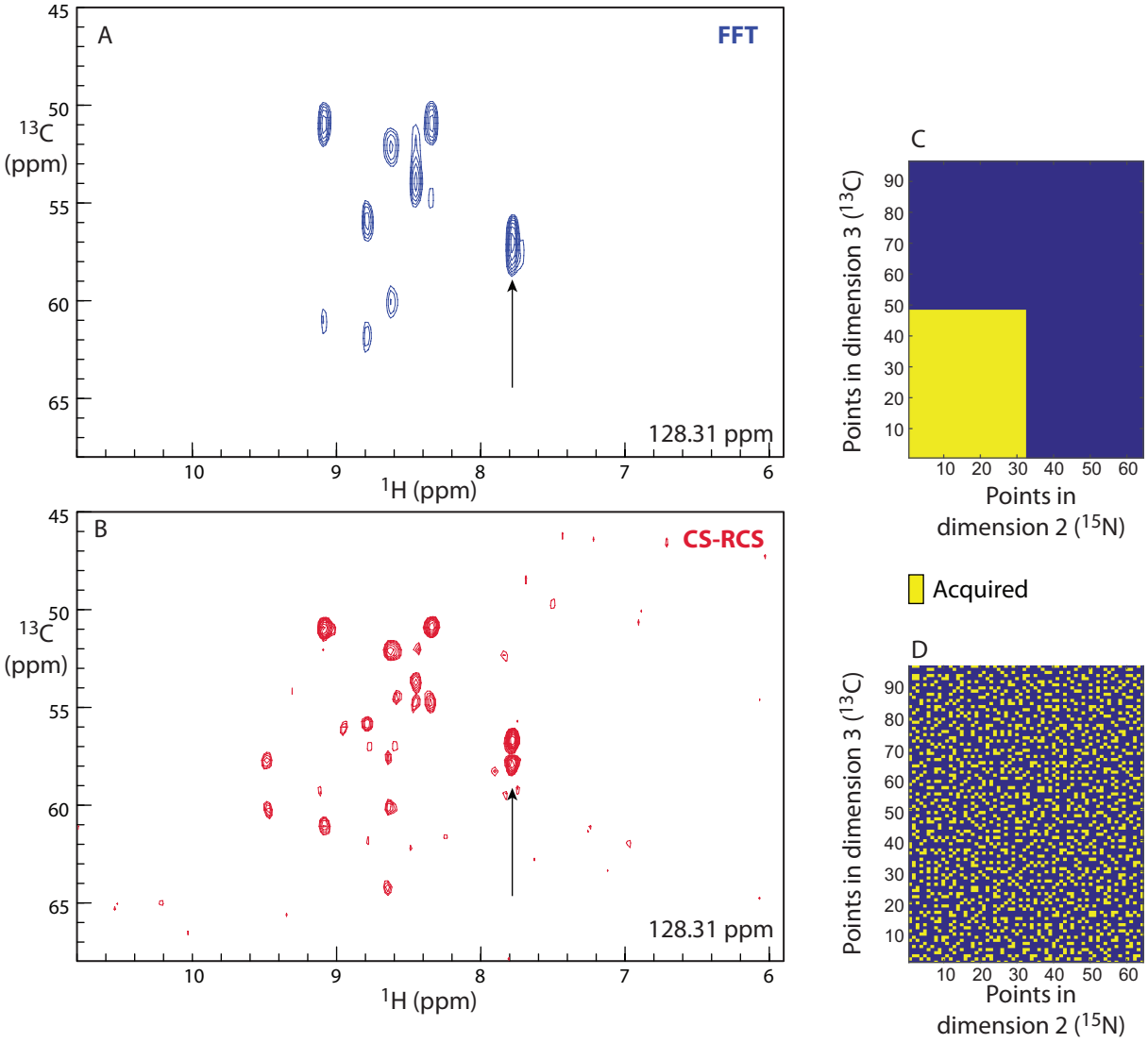

Figure 2. A ^{1}H,^{13}C-plane from a 3D [^{1}H,^{15}N]-TROSY HNCA for *U*-[^{2}H,^{15}N,^{13}C]-labelled S195A-human factor IX, taken at 128.31 ppm in the ^{15}N dimension (dimension 2). In A, FFT reconstruction of fully-sampled data, equivalent to 384 ^{15}N, ^{13}C pairs (1536 total points) or 16 × 24 complex points in the ^{15}N and ^{13}C dimensions respectively is shown. This corresponds to t_{max} for ^{15}N and ^{13}C of 9.22 ms and 5.28 ms respectively. In B, CS reconstruction with RCS in the constant-time ^{15}N dimension and RPD in the ^{13}C dimension is shown. Since this allows a factor of two undersampling in each indirect dimension, i.e. equivalent to 25% sampling, this allows sampling to higher resolution for the same experiment time giving t_{max} of 18.44 ms and 10.56 ms for ^{15}N and ^{13}C respectively. This is equivalent to sampling points from a matrix of 32 × 48 complex points. The reconstruction uses CS-RCS in dimension 2 (^{15}N) and normal CS in dimension 3 (^{13}C). An example of the improved resolution in the CS-RCS spectrum is indicated by a black arrow in A and B. Adjacent to each spectrum, C and D show the region of sampled points, with acquired points indicated. The axes represent total points in each dimension. Data was recorded on a 0.25 mM *U*-[^{2}H,^{15}N,^{13}C]-labelled S195A-human factor IX using a Bruker DRX500 equipped with a 5 mm TCI cryoprobe at 298 K, with 96 scans. The spectral widths in the indirect dimensions were 1736.1 Hz (^{15}N) and 4545.5 Hz (^{13}C).

As before, peak shapes and positions are well recovered.

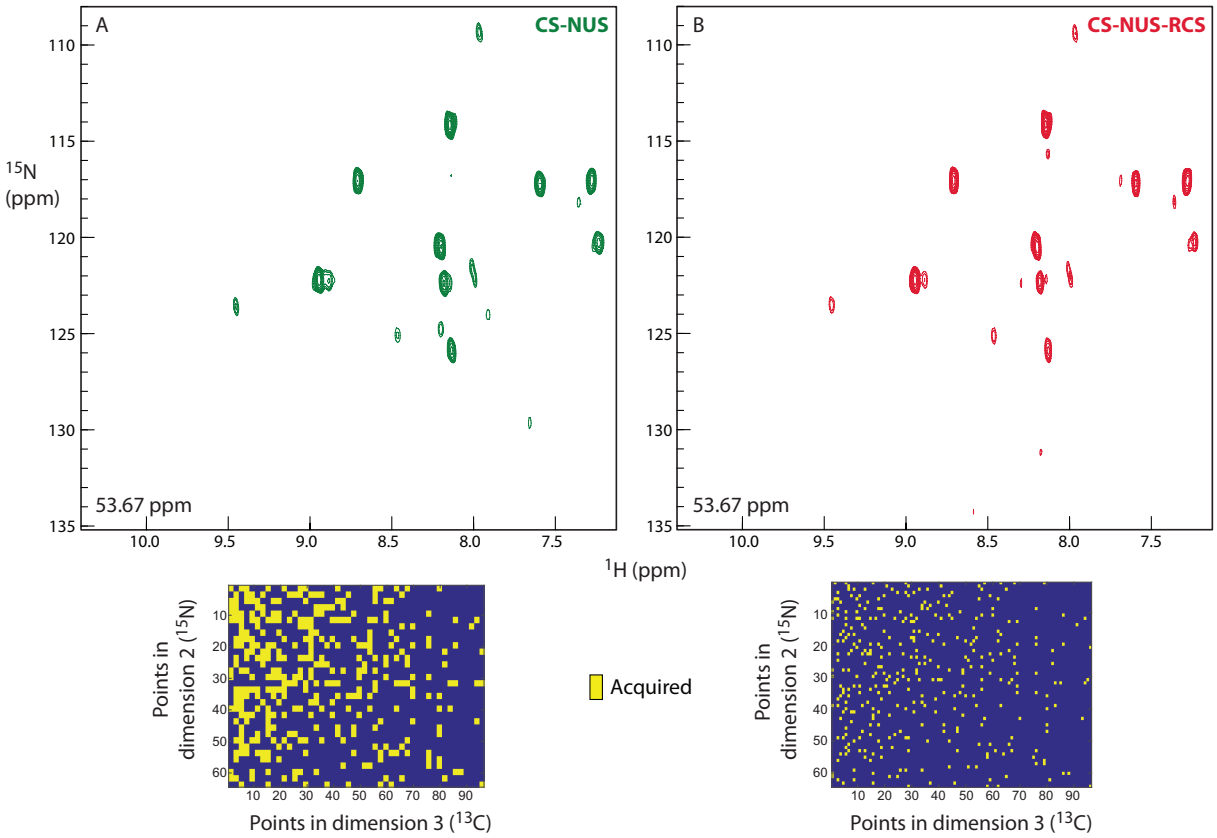

Figure 3. A ^{1}H,^{15}N-plane from the reconstruction of a 3D [^{1}H,^{15}N]-TROSY HN(CO)CA for U-[^{2}H,^{15}N,^{13}C]-labelled S195A-human factor IX, taken at 53.67 ppm in the ^{13}C dimension (dimension 3). In A, CS reconstruction of 22.8% NUS data, equivalent to 350 ^{15}N, ^{13}C complex pairs (1400 total points), giving $t_{1\max}(^{15}N) = 11.52$ ms and $t_{1\max}(^{13}C) = 8.21$ ms, from a fully-sampled matrix of 1536 complex pairs (6144 total points) is shown. In B, CS reconstruction of 5.7% NUS-RPD data, equivalent to 350 points (from 6144 total points) is shown, using CS-RCS reconstruction in dimension 2 (^{15}N) and normal CS-processing in dimension 3 (^{13}C). Sampling schedules for the indirect dimensions are shown below each spectrum, with acquired points indicated. In each case, the resolution is the same, defined by the NUS schedule. RCS and RPD are used here for time-reduction. Data was recorded on a 0.25 mM U-[^{2}H,^{15}N,^{13}C]-labelled S195A-human factor IX using a Bruker AV800 equipped with a 5 mm TXI HCN cryoprobe at 298 K, with 320 scans. The spectral widths in the indirect dimensions were 2777.8 Hz (^{15}N) and 5848.0 Hz (^{13}C).

4. Conclusions

The previously introduced RPD reduces the number of points required for frequency discrimination by a factor of two in each indirect dimension where the data is recorded as cosine and sine components [31]. RCS, introduced in this paper, allows this factor of two saving to be extended into indirect dimensions recorded with gradient selection (P- and N-type data). Both RPD and RCS generate artifacts, similar to NUS. However, processing with CS or MaxEnt can minimise the artifacts from RPD spectra. The adaption of the CS algorithm in this paper, CS-RCS, allows this approach to be applied to minimise the artifacts present in RCS data. This extends the power of RQD to the full suite of experiments available to modern NMR which typically combine indirect dimensions with cosine-/sine- and P-/N-type data. The time savings generated by RQD can be used to enhance resolution, by sampling to higher $t_{\max}$ values in indirect dimensions, or to reduce experiment time in sampling limited regimes. The data shown in this paper demonstrates successful application of these ideas to 2D and 3D experiments.

Since CS processing relies on spectral sparsity, further improvements can be expected for 4D and higher dimensional experiments.

5. Methods

Spectra for the SH3 domain were recorded for a 0.3 mM SH3-domain sample using a 2D [^{1}H,^{15}N]-SOFAST TROSY sequence on a Bruker DRX500 equipped with a 5 mm TCI cryoprobe at 298 K, with 56 complex points in the ^{15}N dimension, $t_{1\max} = 22.1$ ms, and 4 scans. The ^{15}N spectral width was 2530.4 Hz. Recording time for the fully-sampled data was 6 min.

A 0.25 mM *U*-[^{2}H,^{15}N,^{13}C]-labelled S195A-human factor IX sample was used for 3D experiments. The HNCA was recorded on a Bruker DRX500 equipped with a 5 mm TCI cryoprobe with 96 scans and the HN(CO)CA was recorded on a Bruker AV800 spectrometer with 320 scans equipped with a 5 mm TXI HCN cryoprobe, both at 298 K. The full HNCA spectrum was recorded with 16×24 complex pairs in the ^{15}N and ^{13}C dimensions respectively, with spectral widths in the indirect dimensions of 1736.1 Hz (^{15}N) and 4545.5 Hz (^{13}C) and $t_{\max}$ for ^{15}N and ^{13}C of 9.22 ms and 5.28 ms respectively. The HN(CO)CA was recorded as an NUS experiment with 350 complex pairs according to an exponential schedule with spectral widths in the indirect dimensions of 2777.8 Hz (^{15}N) and 5848.0 Hz (^{13}C) and $t_{1\max}$ for ^{15}N and ^{13}C of 11.52 ms and 8.21 ms respectively.

Spectra were reconstructed with Azara (W. Boucher, unpublished) or MATLAB for FT reconstructions and with custom-written MATLAB and Python scripts for CS-processing, using a modified form of the IHT algorithm [25]. NUS schedules were generated using ScheduleTool [38] and RQD schedules using custom-written MATLAB code. Spectra were analysed in Azara and CCPN Analysis [39].

Acknowledgments

Thanks to Dr. Daniel Holland for useful discussions and to Dr. Jennifer Kopanic for the S195A-Factor IX sample.

References

[1] Szyperski T, Yeh D C, Sukumaran D K, Moseley H N B and Montelione G T 2002 *PNAS* **99** 8009
[2] Gautier A, Mott H R, Bostock M J, Kirkpatrick J P and Nietlispach D 2010 *Nat. Struct. Mol. Biol.* **17** 768
[3] Hiller S, Garces R G, Malia T J, Orekhov V Y, Colombini M and Wagner G 2008 *Science* **321** 1206
[4] Kim H J, Howell S C, Van Horn W D, Jeon Y H and Sanders C R 2009 *Prog. Nucl. Magn. Reson. Spectrosc.* **55** 335
[5] Fiaux J, Bertelsen E B, Horwich A L and Wüthrich K 2002 *Nature* **418** 207
[6] Sprangers R, Velyvis A and Kay L E 2007 *Nat. Methods* **4** 697
[7] Barna J C J, Laue E D, Mayger M R and Worrall S J P 1987 *J. Magn. Reson.* **73** 69
[8] Schmieder P, Stern A S, Wagner G and Hoch J C 1994 *J. Biomol. NMR* **4** 483
[9] Coggins B E and Zhou P 2008 *J. Biomol. NMR* **42** 225
[10] Kazimierczuk K, Koźmiński W and Zhukov I 2006 *J. Magn. Reson.* **179** 323
[11] Marion D 2005 *J. Biomol. NMR* **32** 141
[12] Marion D 2006 *J. Biomol. NMR* **36** 45
[13] Hoch J C, Stern A S, Donoho D L and Johnstone I M 1990 *J. Magn. Reson.* **86** 236
[14] Rovnyak D, Frueh D P, Sastry M, Sun Z-Y J, Stern A S, Hoch J C and Wagner G 2004 *J. Magn. Reson.* **170** 15
[15] Orekhov V Y, Ibraghimov I V and Billeter M 2001 *J. Biomol. NMR* **20** 49
[16] Tugarinov V, Kay L E, Ibraghimov I V and Orekhov V Y 2005 *J. Am. Chem. Soc.* **127** 2767
[17] Matsuki Y, Eddy M T and Herzfeld J 2009 *J. Am. Chem. Soc.* **131** 4648
[18] Atreya H S and Szyperski T 2004 *PNAS* **101** 9642
[19] Kupče E and Freeman R 2003 *J. Am. Chem. Soc.* **125** 13958
[20] Candes E J, Romberg J and Tao T 2006 *IEEE Trans. Inf. Theory* **52** 489
[21] Donoho D L 2006 *IEEE Trans. Inf. Theory* **52** 1289
[22] Logan B F 1965 Properties of high-pass signals. PhD thesis, Columbia University, New York.

[23] Holland D J, Bostock M J, Gladden L F and Nietlispach D 2011 *Angew. Chem. Int. Ed.* **50** 6548
[24] Kazimierczuk K and Orekhov V Y 2011 *Angew. Chem. Int. Ed.* **50** 5556
[25] Bostock M J, Holland D J and Nietlispach D 2012 *J. Biomol. NMR* **54** 15
[26] Hyberts S G, Milbradt A G, Wagner A B, Arthanari H and Wagner G 2012 *J. Biomol. NMR* **52** 315
[27] Kazimierczuk K and Orekhov V Y 2012 *J. Magn. Reson.* **223** 1
[28] Sun S, Gill M, Li Y, Huang M and Byrd R A 2015 *J. Biomol. NMR* **62** 105
[29] Marion D and Wüthrich K 1983 *Biochem. Biophys. Res. Commun.* **113** 967
[30] States D, Haberkorn R and Ruben D 1982 *J. Magn. Reson.* **48** 286
[31] Maciejewski M W, Fenwick M, Schuyler A D, Stern A S, Gorbatyuk V and Hoch J C 2011 *PNAS* **108** 16640
[32] Keeler J and Neuhaus D 1985 *J. Magn. Reson.* **63** 454
[33] Davis A L, Keeler J, Laue E D and Moskau D 1992 *J. Magn. Reson.* **98** 207
[34] Hoch J, Maciejewski M and Filipovic B 2008 *J. Magn. Reson.* **193** 317
[35] Delsuc M A 1988 *J. Magn. Reson.* **77** 119
[36] Musacchio A, Noble M, Pauptit R, Wierenga R and Saraste M 1992 *Nature* **359** 851
[37] Johnson D J D, Langdown J and Huntington J A 2010 *PNAS* **107** 645
[38] Maciejewski M W and Gorbatyuk V Sample Scheduler for Non-Uniform Data Sets `http://sbtools.uchc.edu/nmr/sample_scheduler/`
[39] Vranken W F, Boucher W, Stevens T J, Fogh R H, Pajon A, Llinas M, Ulrich E L, Markley J L, Ionides J and Laue E D 2005 *Proteins* **59** 687